THE PHYSICAL THEORY OF ONE-DIMENSIONAL GALACTIC COSMIC-RAY PROPAGATION IN THE ATMOSPHERE

Keran O'Brien

Health and Safety Laboratory, U. S. Atomic Energy Commission, New York, N. Y.

An essentially analytical theory of atmospheric cosmic-ray propagation is developed on the basis of a phenomenological model of hadron-nucleus collisions. This model correctly predicts the sea-level cosmic-ray nucleon, pion and muon spectra, the cosmic-ray ionization profile in the atmosphere, and neutron flux and density profiles in the atmosphere. It is concluded that the large scale properties of atmospheric cosmic-rays can be accurately predicted on the basis of a purely nucleonic cascade as a result of which all secondaries are mediated by pion production.

Implications for energy independence of cross sections, the recent 70 GeV results from Serpukhov, and nucleonic relaxation rates in the atmosphere are discussed.

INTRODUCTION

This paper attempts to establish the physics on which the large-scale, time-averaged, one-dimensional properties of galactic cosmic-rays in the atmosphere depend.

The point of departure for this theory is a phenomenological model of high energy nucleon-nucleus collisions which can be applied to analytical transport theory. Particle spectra, fluxes, densities and ionization calculated from the theory yield good agreement with measured values indicating the adequacy of the nuclear model and of the supporting cosmic-ray and geophysical data. All comparisons are on an absolute basis.

Preliminary results of this work have already been reported comparing calculations and measurements of various components of cosmic-ray ionization in the lower atmosphere (<2.5 km elevation) at a geomagnetic latitude of $51°$ (ref. 1).

ATMOSPHERIC MODEL

The atmosphere is assumed to be a flat slab 1033 g/cm^2 thick with a constant scale height of 6.7 km. It is assumed to be composed of a single nuclear species with an atomic weight of 14.48, atomic number of 7.31, and an ionization potential of 86.8 volts. Because oxygen and nitrogen are so close in the periodic table, this simple assumption yields the correct nuclear data. The density of the atmosphere is

$$\rho = r/H \qquad (1)$$

where

ρ is the density in g/cm^3,

r is the depth in the atmosphere in g/cm^2, and

H is the scale height in cm.

Since the mean free path for decay of a charged particle is

$$\lambda_q = \frac{(P_q c)}{(m_q c^2)} \, (c\tau_q \rho) \qquad (2)$$

where

λ_q is the mean free path for decay in g/cm^2 of a particle of type q,

m_q is the mass of the particle in MeV/c^2,

P_q is the momentum in MeV/c,

c is the velocity of light, and

τ_q is the mean life in the rest frame, in seconds,

we have the useful result that

$$\lambda_q = P_q cr/C_q, \qquad (3)$$

where

$$C_q = m_q c^2 H/c\tau_q.$$

THEORY OF THE ATMOSPHERIC NUCLEONIC CASCADE

The Boltzman Equations

In this paper, atmospheric cosmic-ray fluxes will be obtained as analytic solutions to an approximate form of the Boltzman equations. The Boltzman equations for the nucleonic cascade in the atmosphere are

$$B_q \varphi_q(r,E,\vec{\Omega}) = S_{qj}, \qquad (4.1)$$
$$(q = p,n,\pi : j = p,n),$$

$$B_\mu \varphi_\mu(r,E,\vec{\Omega}) = S_{\mu\pi^\pm},$$

$$B_\alpha \varphi_\alpha(r,E,\vec{\Omega}) = S_{\alpha\beta},$$
$$(\alpha = \gamma, e : \beta = \gamma, e, \pi^0, \mu),$$

$$B_q = \vec{\Omega} \cdot \nabla + \sigma_q + \frac{C_q}{P_q cr} - \frac{\partial}{\partial E} k_q$$
$$(q = p,n,\pi,\mu,e\gamma), \qquad (4.2)$$

$$S_{qj} = \int_{4\pi} d\vec{\Omega}' \int_E^\infty dE_B \, \sigma_{qj} \, F_{qj}(E_B \rightarrow E, \vec{\Omega}' \cdot \vec{\Omega}').$$
$$\cdot \varphi_j(r, E_B, \vec{\Omega}') \qquad (4.3)$$

$(qj = np, pn, \pi n, \pi p, \mu\pi^\pm, e\mu, \gamma\pi^0, e\gamma, \gamma e),$

$$\sigma_\mu = C_p = C_n = C_e = C_\gamma = k_n = k_{\pi^0} = k_\gamma = 0,$$

where

r is the depth in the atmosphere in g/cm^2,

E is the particle kinetic energy in MeV,

$\vec{\Omega}$ is the unit vector in the direction of particle travel,

φ_q is the particle flux of type q per second per steradian at a depth r with a direction $\vec{\Omega}$,

σ_q is the total cross section for absorption of a particle of type q in cm^2/g,

σ_{qj} is the cross section for the production of particles of type q from collisions with, or decay by, particles of type j in cm^2/g,
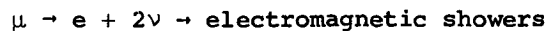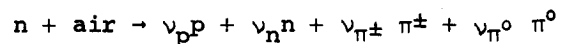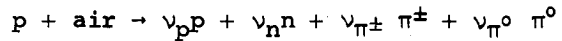
k_q is the stopping power of a charged particle of type q in air, in $MeV \, cm^2/g$, and

F_{qj} is the number of particles per MeV per second per steradian at E and Ω resulting from a collision with or decay by a particle of type j at E_B and $\vec{\Omega}'$.

The subscript π implies application to all pions, charged and neutral. The subscript $\pi^\pm$ implies application to the charged pions, and π^0 to neutral pions only.

Nucleon-Nucleus Collisions

In eq. (4) it has been assumed that atmospheric cosmic-rays propagate by means of the nucleonic cascade in an exponential atmosphere [see Fig. 1 of O'Brien (ref. 1)]. Thus all other secondaries result from nucleon-nucleus collisions. The following reactions are considered.

$$p + air \rightarrow \nu_p p + \nu_n n + \nu_{\pi^\pm} \pi^\pm + \nu_{\pi^0} \pi^0$$

$$n + air \rightarrow \nu_p p + \nu_n n + \nu_{\pi^\pm} \pi^\pm + \nu_{\pi^0} \pi^0$$

$$\pi^\pm \rightarrow \mu + \nu \qquad (5)$$

$$\pi^0 \rightarrow 2\gamma \rightarrow \text{electromagnetic showers}$$

$$\mu \rightarrow e + 2\nu \rightarrow \text{electromagnetic showers}$$

where ν_j are the multiplicities of j type resulting from the collision of a nucleon with a nucleus of air. The influence of kaon production has earlier been shown to have a small influence on ionization, and it is neglected here, at a considerable saving of computer time (ref. 1).

The nucleon-nucleus reactions of eq. (5) will be considered at high energies only, because the mathematical form of the approximation to the Boltzman equation to be obtained is only applicable at energies above about 0.1 GeV*.

It is required (a foreseen mathematical result motivates the choice of the function) that

$$G_{qj} = I_q \frac{E_B^{\ell}}{E^n} U(E_B - \eta_q)$$

$$G_{qj} = 2\pi \int_o^{\pi} d\theta \sin\theta \, F_{qj}(E_B \to E, \Omega) \quad (6)$$

$$\Omega = \cos\theta$$

where

G_{qj} is the secondary production spectrum of type q particles integrated over the solid angle,

I_q is an arbitrary constant depending on q,

ℓ and n are arbitrary constants which must be the same for all j,q, and

$U(x)$ is the Heaviside function [$U(x < 0) = 0$, $U(x \geqq 0) = 1$],

η_q is a lower energy limit below which secondary particle production is cutoff.

The formula for G_{qj} is certainly very crude, however it is suitable to represent the behavior of the partial inelasticities and multiplicities associated with high energy nucleon-nucleus collisions. Inelasticities are known to vary quite slowly with energy, and to become essentially constant at energies of a few 10's of GeV (ref. 2). If $n = \ell + 1$, then G_{qj} can be rewritten in terms of a constant partial inelasticity, K_q, for the production of a type q particle

$$G_{qj} = (1 - \ell) K_q \frac{E_B^{\ell}}{E^{1+\ell}} U(E_B - \eta_q) \quad (7)$$

Hagedorn and Ranft (ref. 3) have calculated K_q using the statistical model for p-p collisions at 12.5, 18.8, 30 and 300 GeV/c and it would be quite convenient to use these results for K_q. However, Alsmiller and Barish (ref. 4) have shown that the secondary production spectrum,

G_{qj}, softens with increasing atomic weight as a result of the intranuclear cascade. This effect has been simulated in eq. (7) by making K_q a function of atomic weight (ref. 5). This is, unfortunately, at the expense of the conservation of energy in high atomic weight nuclei, although for air, energy is conserved reasonably well. The intranuclear cascade conserves energy as G_{qj} softens, by the emission of low energy particles but these low energy particles are not important to deep penetration calculations at high energies. Values of K_q interpolated from among the values obtained earlier are given in Table I (ref. 5).

Table I. - Partial inelasticities for proton-air collisions.

q	K_q
p	0.211
n	0.211
π^+	0.180
π^-	0.112
π^o	0.180
K^+	0.034
K^-	0.022
K^o	0.034

Experimental values of partial inelasticities in the energy range 0.1 to 20 TeV have been obtained in nuclear emulsion from the Brawley and I.C.E.F. emulsion stacks (ref. 2). The quantities measured were; K_{ch}, the energy that goes into new charged particles, and hence

$$K_{ch} = K_{\pi^+} + K_{\pi^-} + K_{K^+} + K_{K^-}; \quad (8)$$

K_γ is the energy that goes into photon production, and so

$$K_\gamma = K_{\pi^o}; \quad (9)$$

K_o is the energy that goes into long lived neutral particles. It is assumed that these are neutral kaons. This is a small number, and any error that may arise here is unimportant to the study. The energies involved in the measurement are high compared to the largest rest masses involved and thus they may be neglected.

*Low energy nucleon transport (<0.1 GeV) is chiefly neutron transport. Low energy neutron and electromagnetic shower transport are treated only very roughly here due to the limitations of the transport theory to be described. It is intended in the near future to apply the S_n method to this problem, and treat it much more generally. The analytic theory presented here is if less general, quite accurate at high energies, quite simple and rather transparent.

In Table II, the predictions of O'Brien (ref. 5) (which in conjunction with eq. (7) will be referred to as the power law model hereafter) is compared with these data, and with the predictions of other nuclear models.

These other nuclear models have all been compared against, and in some cases based upon, accelerator target yields, mostly at small angles and at high secondary momenta. The well known CKP model (ref. 6), the Trilling model (ref. 7), the extrapolation model (ref. 8), and the TRB model (ref. 9) are considered. Ranft and Borak (ref. 9) have modified the formulae used by Trilling (ref. 7), and this is referred to as the TRB model.

Table II. - Partial inelasticities at very high energies.

	Experimental[a] (0.1-20 TeV)	Statistical[B] model (300 GeV)	Power Law[a] model (=)	TRB[C] model (20 GeV)	Extrapolation[b] model (200 GeV)	Trilling[B] model (=)	CKP[B] model
K_{ch}	0.31± .06	0.364	0.303	0.23	0.166	0.21	0.38
K_γ	0.16	0.186	0.157	0.14	0.084	0.09	-
K_0	0.03	0.035	0.029	-	-	0.01	-
Total	0.50±0.07	0.585	0.489	-	-	0.31	-

a nuclear emulsion.

B hydrogen.

c air, kaons neglected.

b aluminum, kaons neglected.

The considerable variation is occasion for surprise. The statistical model, the power law model which is an adaption of it, and the CKP model are in agreement with the cosmic-ray emulsion measurements, though all the models appear to agree within a factor of two. This is probably a consequence of the fact that most of the accelerator target data, and much of the physical interest, is at small forward angles and at large secondary momenta, and this does not determine K_q precisely enough.

The secondary particle multiplicities of the power law model depend on the value chosen for ℓ. Since eq. (7) has an "infrared" divergence, it it not suitable for total particle yields. However, shower particles in an emulsion produced by high energy nucleons have finite lower energy limits of 80 MeV for mesons and 500 MeV

for protons (ref. 10). The power law model yields as the multiplicity of particles above a lower limit Γ

$$\nu_q(E_B) = [(1 - \ell)/\ell]K_q[(E_B/\Gamma)^\ell - 1].$$

Using the data of Meyer et al. (ref. 11), the best value of ℓ, in the least squares sense, was chosen. The procedure is described in a somewhat more expanded way in O'Brien (ref. 5). In Table III, the predictions of shower particle production by various nuclear models are given. The power law result is not really a prediction but a fit. Since the statistical model and the extrapolation model cannot be manipulated without the proper computer codes, their reported total charged particle production is given in place of the shower particle multiplicities. As the Trilling model does not give back emitted particles correctly (ref. 7) it has been omitted from consideration here.

Some of the differences in Table III are certainly due to differences in the target nucleus and in the lower energy limit. But it is clear that the power law model agrees with the experimental data as well as the other models.

Multiplicities and inelasticities are averaged quantities related to hadron-nucleus collisions. Matters are different when one considers the form of G_{qj} predicted by the various models. Figure 1 exhibits $G_{\pi\pm p}(E_B, E)$ for E_B equal to 10 and 100 GeV protons incident on air calculated using the power law and TRB prescriptions, and the CKP prescription for protons on hydrogen. The CKP and TRB models agree at high secondary momenta, but differ elsewhere. The greater sophistication of the TRB model can be seen in the graph. For instance, the inflection point at $G_{\pi\pm p}(100, 18)$ corresponds to the transition from energetic pions resulting from isobar decay to low energy pions emitted isotropically in the center of mass. The power law model overestimates pion production at high secondary momenta but underestimates at low secondary momenta.

In Fig. 2, secondary proton production predictions $G_{pp}(E_B, E)$ are exhibited for protons on air, again for E_B equal to 10 and 100 GeV. The relative crudity of the power law model is clear. It underestimates proton production at high secondary momenta and overestimates at low secondary momenta. It is probably more significant for the cascade
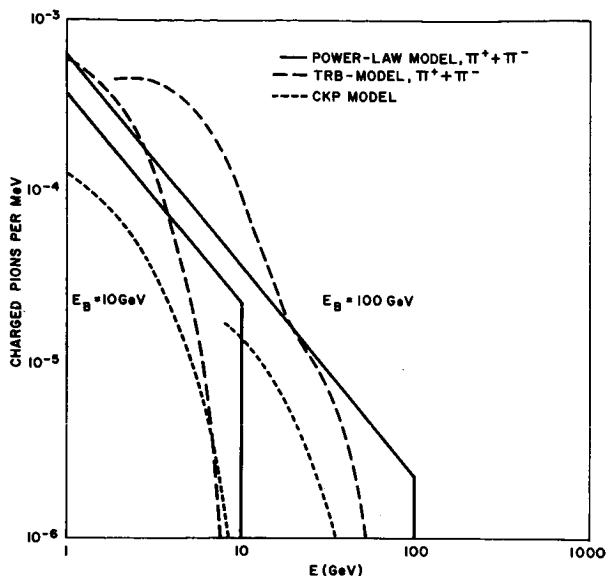
Fig. 1. Three models of charged pion production spectra from proton-air collisions.
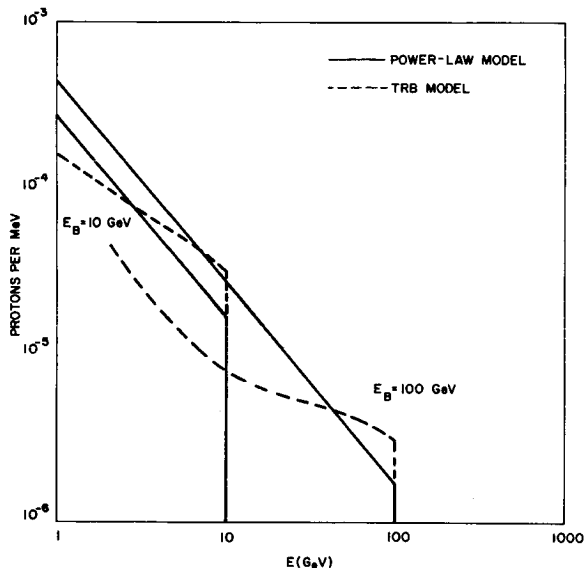

Figure 2. Two models of proton production spectra from proton-air collisions.

APPROXIMATE SOLUTION TO THE BOLTZMAN EQUATIONS

Hadrons and Muons

A solution will be obtained for a sort of "Green's function", that is for incident nucleons homogeneous in energy and angle, of unit strength per steradian, the integral of which over the cosmic-ray primaries yields atmospheric cosmic-ray fluxes per steradian per second.

Making the "straight-ahead" approximation

$$F_{qj} = G_{qj} \; \delta \; \frac{(1 - \vec{\Omega}' \cdot \vec{\Omega})}{2\pi} \qquad (11)$$

and eq. (4.3) becomes for the hadron component

$$S_{qj} = \int_{E}^{E_0} dE_B \; \sigma \; G_{qj}(E_B, E)\varphi_j(r, E_B, \Omega)$$

$$(qj = np, pn, \pi n, \pi p) \qquad (12)$$

where σ is the geometric reaction cross section in cm^2/g, and for the muons (ref. 13)

$$S_{\mu\pi\pm} = \frac{m_{\pi\pm}/m_\mu}{2\pi} \cdot \frac{C_{\pi\pm}}{P_{\pi\pm} \; r} \; \varphi_{\pi\pm}[r(m_{\pi\pm}/m_\mu) E_B, \Omega] \qquad (13)$$

where Ω is the cosine of the zenith angle of the incident radiation and E_0 is the energy of the incident nucleon.

The Boltzman operator of eq. (4.2) for the muon component is then

$$B_\mu = \Omega \frac{\partial}{\partial r} + \frac{C_\mu}{P_\mu \; r} - \frac{\partial}{\partial E} k_\mu. \qquad (14.1)$$

The neutron operator is

$$B_n = \Omega \frac{\partial}{\partial r} + \sigma \qquad (14.2)$$

The remainder are all simplified by the omission of charged particle stopping

$$B_p = \Omega \frac{\partial}{\partial r} + \sigma \qquad (14.3)$$

$$B_\pi = \Omega \frac{\partial}{\partial r} + \sigma + \frac{C_\pi}{P_\pi \; r} \qquad (14.4)$$

This omission is not important for secondaries above about 1 GeV (ref. 14). Compensation for this can roughly be made with the use of the Heaviside function of eq. (7), as will be shown.

Separating the primary nucleons from the secondaries produced in the atmosphere

$$\varphi_q = \varphi_{iq} + \varphi_{sq} \qquad (15)$$

calculations to follow that the power law model should be right on the average, than it should be right at some particular secondary energy or angle.

The reaction cross sections used in the calculation to follow are assumed to be constant and geometric, i.e. $\sigma = \pi r_0^2 \; L/A$, $r_0 = 1.28 \; A^{\frac{1}{3}} \; F$, where L is Avogadro's number. This assumption is valid for low energy nucleon-nucleus collisions for atomic weights from less than 12 to greater than 64 (ref. 12), and it is used in what follows for all energies and hadrons.

Table III. - Shower particle multiplicities.

E (GeV)	Experimental[a]	Power Law[a] model	Statistical[b] model	Extrapolation[c] model	TRB[d] model	CKP[e] model
12.5	3.8	5.0	3.0	5.5	3.8	4.9
20	5.3	5.9	3.8	-	4.3	5.5
30	7.3	6.8	4.8	-	5.0	6.1
200	12	12	-	6.9	10	9.8
300	13	13	8.5	-	12	11
1000	17	17	-	-	20	15

[a] nuclear emulsion.

[b] hydrogen, total charged particle yield.

[c] aluminum, total charged particle yield, kaons neglected.

[d] air, kaons neglected.

[e] hydrogen, total charged pion yield.

where

φ_{iq} is the flux of primary nucleons, and

φ_{sq} is the flux of secondary nucleons.

This leads to 3 differential equations

$$\left[\Omega \frac{\partial}{\partial r} + \frac{C_\mu}{P_\mu r} - \frac{\partial}{\partial E} k_\mu\right]\varphi_{s\mu} = \frac{m_{\pi\pm}}{2\pi m_\mu} \cdot$$

$$\cdot \frac{C_{\pi\pm}}{P_{\pi\pm} r} \varphi_{s\pi\pm} \left(r, \frac{m_{\pi\pm}}{m_\mu} E_B, \Omega\right) \qquad (16.1)$$

$$\left[\Omega \frac{\partial}{\partial r} + \sigma\right]\varphi_{iq} = 0 \qquad (q = p, n) \qquad (16.2)$$

$$\left[\Omega \frac{\partial}{\partial r} + \sigma + \frac{C_q}{P_q r}\right]\varphi_{sq}$$

$$= \sum_{j=p,n} \int_E^{E_{max}} dE_B \, \sigma(1 - \ell) K_q \cdot$$

$$\cdot \frac{E_B^\ell}{E^{1+\ell}} U(E - \eta_q) \qquad (q = p,n,\pi) \qquad (16.3)$$

Equation (16.1) is written in integral form and reduced to quadratures (ref. 15). A 51 point set was found necessary for the integral over space and 7 for the integral over angle.

The solution to eq. (16.2) is

$$\varphi_{iq} = \exp(-r/\sigma\Omega) \qquad (17.1)$$

Passow (ref. 16), and Alsmiller (ref. 17) have shown that the solution to an integro-differential equation of the form of equation (16.3) with constant cross section for incident nucleon flux of energy E_0 and zenith direction Ω is

$$\varphi_{sq} = \frac{\sigma^2}{\left(\sigma + \frac{C_q}{P_q r}\right)} (1 - \ell) K_q \left(\frac{E_0^\ell}{E^{1+\ell}}\right) \cdot$$

$$\cdot U(E_0 - \eta_v) \left[\frac{r}{\Omega B(E_0, E)}\right]^{\frac{1}{2}} \cdot \qquad (17.2)$$

$$\cdot I_1 \left[2\sqrt{(r/\Omega) B(E_0, E)}\right]$$

$$B(E_0, E) = \sigma \sum_{t=n,p} (1 - \ell) K_t \cdot$$

$$\cdot \{\ln E_0 - \ln[EU(E - \eta_t) + \eta_t U(\eta_t - E)]\},$$

$$(v = p,n: q = p,n,\pi)$$

Equation (17.2) differs slightly from the form obtained by Passow (ref. 16) and Alsmiller (ref. 17) by the inclusion of the decay term in the solution. The reason for this lies in the fact that $C_n = C_p = 0$, that $G_{\pi j}$ does not appear under the integral of eq. (16.3), and that pion production and absorption is purely local so that the energy independence of the cross section required by the solution can be relaxed.

The remaining parameter, η_q, is a lower energy limit beneath which secondary particles of type q are suppressed. Thus, $\eta_\pi = E_0$, and $\eta_n = 0$. To compensate for the neglect of proton stopping, η_p is set equal to 500 MeV.

The neglect of charged particle stopping, the straight ahead approximation, and the constant geometric cross section make eq. (17) increasingly shaky as secondary particle energies go below 1 GeV and fails completely by 100 MeV. At high energies, eq. (17) should become and remain quite accurate as long as ℓ and σ can be treated as constants. It may seem that the neglect of hadron production by incident pions should fail at high energy since $\lambda_{\pi\pm}$ (eq. 3) can become very long. However, as argued by Adair (ref. 18), any pion which interacts with a nucleus can be treated as an absorption. This arises because of the combination of the relatively low pion inelasticity with the steepness of the nucleonic energy spectrum. Only rarely will a pion be emitted from a pion-nucleus collision with an energy near to that of the incident nucleon (see Fig. 1 for the predictions of CKP and TRB at high secondary energies). The steepness

of the energy distribution then causes the number of pions resulting from pion-nucleus collisions to be small compared with those produced directly in nucleon-nucleus collisions.

The restrictions on the form of G_{qj} imposed by the power law model would seem _a priori_ to be the most serious limitation on the use of eq. (17). It is then worth pointing out that eq. (17), suitably modified, has been applied to accelerator beam measurements in iron for proton energies from 1 to 18 GeV (refs. 5, 19), and an 8 GeV pion beam on tin (ref. 20) with excellent results.

Once it is established that the parameters underlying the power law model are correct and that the cross sections are correct, more general methods can be used and many of the approximations made here to stay within the bounds of Passow's mathematical framework (refs. 16, 17) can be abandoned. The relative ease and transparency of Passow's approximation make it of value in itself however.

Photons and Electrons

Electromagnetic shower propagation is not so problematic as nucleon transport. Essentially exact Monte-Carlo treatments exist and have been tested against experimental data (ref. 21, 22). These calculations are difficult to carry out over the range of depths and energies required, and as the goal at this time is the establishment of sufficient conditions to determine the atmospheric flux, the propagation of the electromagnetic cascade is treated very primitively.

Since the mean life of the neutral pion is 0.91×10^{-16} s, $\frac{C_{\pi^0}}{\text{Pr}}$ is huge compared with σ ($C_{\pi^0} = 3.3 \times 10^{10}$ GeV) it decays immediately into 2 photons. The muon decay probability is very much less ($C_\mu = 1.1$ GeV) and is of significance only below about 10 GeV. Energy deposition is calculated from the assumption that the total energy of the neutral pion produced per gram of air (from eq. 17.2) is absorbed at the point of production, and 1/3 the total energy of the decaying muon (from eq. 16.1) is absorbed at the point of decay.*

---

*However, at this time, an attempt is being made to apply the electromagnetic shower code CASCADE (ref. 22) to this problem to improve the treatment of this important component of atmospheric cosmic rays.

This assumption will deteriorate inversely as geomagnetic latitude. As the geomagnetic cutoff rises toward 17 GV, the neutral pion production spectrum will become harder, and as the radiation length of air is of the same order of magnitude as the nucleonic collision mean free path, neglect of transport will become increasingly serious. However at higher latitudes, the error will be seen to be tolerable.

SOLAR AND TELLURIAN MODIFICATION OF THE GALACTIC COSMIC-RAY SPECTRUM

Solar Activity and the Interplanetary Medium

It is well known that variations of solar activity, through the agency of the solar wind modulates the cosmic-ray spectrum found at the earth's orbit. This modulation is a consequence of cosmic-ray transport through the interplanetary medium and it is formally the same as that which would be produced by a heliocentric electric field having a magnitude at the earth's orbit of about 100 MV at solar minimum and about 1000 MV at solar maximum (ref. 23, 24).

The electric field model is a useful computational tool for representing solar effects as the potential is the only adjustable parameter. This representation is for convenience only. It is not asserted here that a heliocentric potential of this size exists and is responsible for solar modulation.

The electric field model of the modulated cosmic-ray flux is (ref. 25)

$$n(E) = n_0(T) \left[\frac{P(E)}{P(T)}\right]^3 \left[\frac{W(T)}{W(E)}\right], \qquad (18)$$

$$T = E + ZU$$

$$P(x) = \frac{1}{c} \sqrt{x^2 + 2A \, m_p \, c^2 \, x},$$

$$W(x) = x + A \, m_p \cdot c^2$$

where

n_0 is the unmodulated galactic spectrum of atomic weight A, and atomic number Z, per steradian per cm^2 per s per MeV, having an energy of E MeV, and

U is the solar potential in MV.

For the calculations to follow, the unmodulated spectrum is taken from Freier and Waddington (refs. 24, 26) below 10 GeV per nucleon. Above that energy the

932

spectrum is taken from Peters (ref. 27) with which it has a smooth overlap.

Calculations of atmospheric ionization will be made and compared with some of the measurements performed by Neher (ref. 28). These measurements have been analyzed to yield the incident proton cosmic-ray spectrum. This is compared to the predictions of the electric field model for U = 200 MeV in Fig. 3. The measurements were performed during the course of several months in 1965, and are near a solar minimum, but a minimum not as deep as that of 1954 (ref. 28), so the value of U is reasonable. The agreement is quite good, and this spectrum will be used for the ionization calculations to follow. Some neutron calculations will require different values of U. These will be taken, where possible, from Freier and Waddington (ref. 26).

In Fig. 4 the cutoffs for the eastern and western horizons and the zenith, from Lemaitre and Vallarta (ref. 30) are shown along with the values obtained by Richtmeyer et al. (ref. 29) as a function of geomagnetic latitude. It is evident that the assumption of isotropy of the radiation near cutoff is not justified at latitudes below 40° to 45°.

This, in combination with the assumptions made with respect to electromagnetic shower transport, will probably cause the calculations based on an isotropically incident spectrum to fail at low latitudes. Consequently, at this stage in the development of the calculations the experimental comparisons will be limited to higher latitudes.
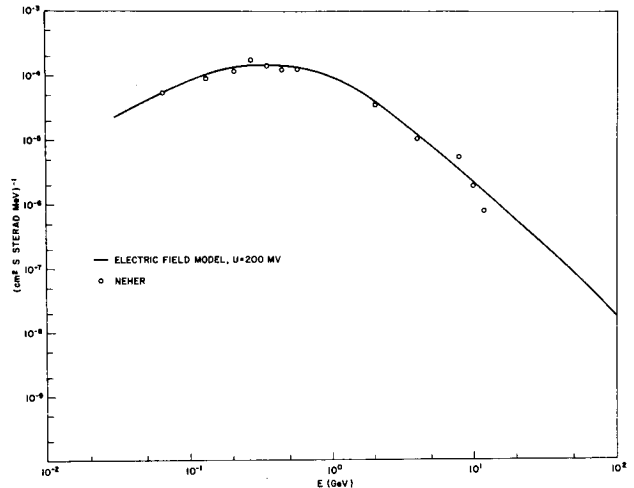

Fig. 3. The East-West variation of geomagnetic cutoff rigidity as a function of geomagnetic latitude compared with the effective cutoff rigidity for an isotropic detector.

Fig. 4. Comparison of electric field model calculations of the incident cosmic-ray proton spectrum with Neher's measurements.

The Earth's Magnetic Field

The magnetic field of the earth deflects incoming cosmic-rays depending on their rigidity and angle of incidence, so that for each angle of incidence there is a critical rigidity below which the incoming particle cannot interact with the earth's atmosphere. In the calculations which follow, a single cutoff rigidity will be applied. The primary spectrum will be assumed unchanged in angle and energy above the cutoff, and vanish below it. Richtmeyer et al. (ref. 29) have calculated the effective cutoff rigidity seen by an isotropic detector exposed to the primary spectrum at the top of the atmosphere and this cutoff will be used here.

COMPARISON WITH EXPERIMENT

Sea-Level Particle Spectra

The first step in producing integral quantities such as ionization or neutron density is the calculation of the differential energy angle particle distributions.

As a test of eq. (17), the vertical component of the cosmic-ray spectra has been calculated for a geomagnetic latitude of 57°. Equation (17) with $\Omega = 1$ and r = 1033 g/cm^2, was integrated over the source spectrum. Seventy percent of the source spectrum was assumed to be composed of free protons, and 30 percent of bound neutrons and protons all having

the energy distribution given by eq. (18), with U = 200 MV. For geomagnetic purposes bound nuclei were treated as bound, but for the purpose of atmospheric transport treated as free i.e., an α particle is assumed to behave exactly like 2 free neutrons and 2 free protons. In Fig. 5, the calculated vertical component of the cosmic-ray nucleon spectrum of one charge state (neutrons or protons) is compared with the experimental sea level proton spectrum of Brooke and Wolfendale (ref. 31) and the sea level neutron spectrum of Ashton and Coats (ref. 32).

At this atmospheric depth, eq. (17) predicts nearly equal numbers of neutrons and protons, and so both experimental and theoretical data were combined. Agreement is very good over 4 decades of energy and 10 of intensity.

The calculated vertical component of the sea level pion spectrum is compared in Fig. 6 with the measurements of Brooke et al. (ref. 33). Agreement is good over most of the range of comparison.

The sea level muon spectrum for a zenith angle of 0° is shown in Fig. 7 compared with measurements by Owen and Wilson (ref. 34), Holmes et al. (ref. 35), Gardener et al. (ref. 36) and Hyman and Wolfendale (ref. 37). Agreement with experiment is quite satisfactory over the range from about 1 to about 1000 GeV. All measurements and calculations were for 57° geomagnetic latitude.

Fig. 6. The vertical component of the cosmic-ray pion flux as measured by Brooke et al. (ref. 33), and as calculated.
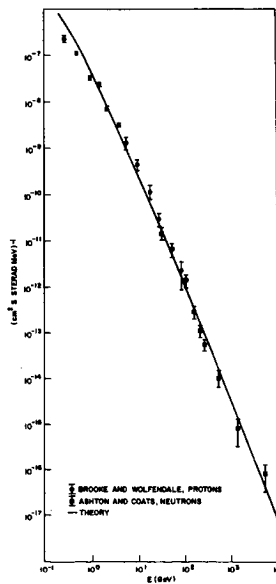

Fig. 5. The vertical component of the cosmic-ray nucleon flux of one charge state at sea level as measured by Brooke and Wolfendale (ref. 31), by Ashton and Coats (ref. 32), and as calculated.
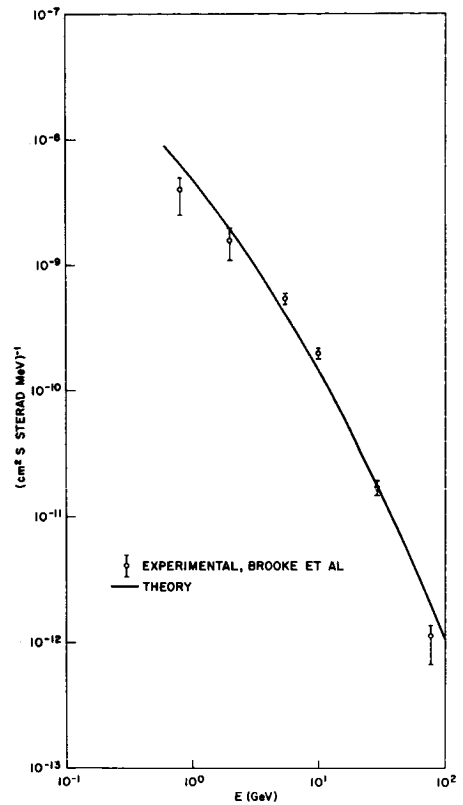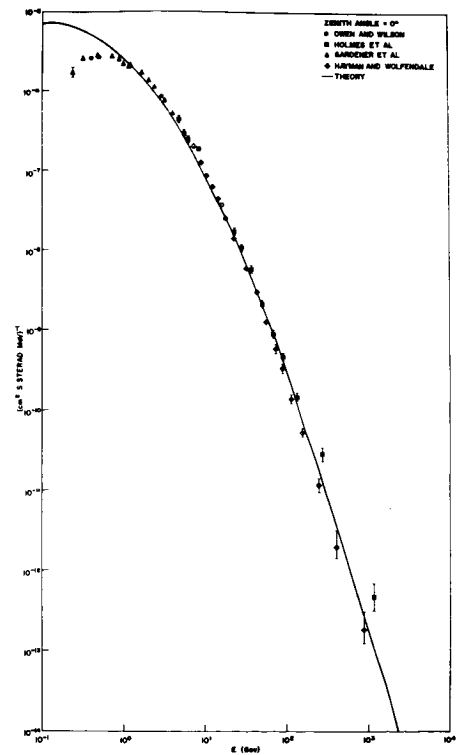

Fig. 7. The vertical component of the cosmic-ray muon flux as measured by Owen and Wilson (ref. 34), Holmes et al. (ref. 35), Gardener et al. (ref. 36), and Hayman and Wolfendale (ref. 37), and as calculated.

In Fig. 8, the sea-level muon spectrum is calculated for a zenith angle of 75° and compared with the measurements of Stefanski et al. (ref. 38). The lowest experimental point is above the maximum cutoff for this latitude, 52° (see Fig. 4).

As has been observed earlier, the assumptions that lead to eq. (17) become increasingly shaky below about 1 GeV. This affects all the charged particle distribution, including the muon energy distribution which of course depends on the pion distribution, and can be seen clearly in Fig. 5, 6, and 7, where the calculated fluxes rise above the measured fluxes in every case.
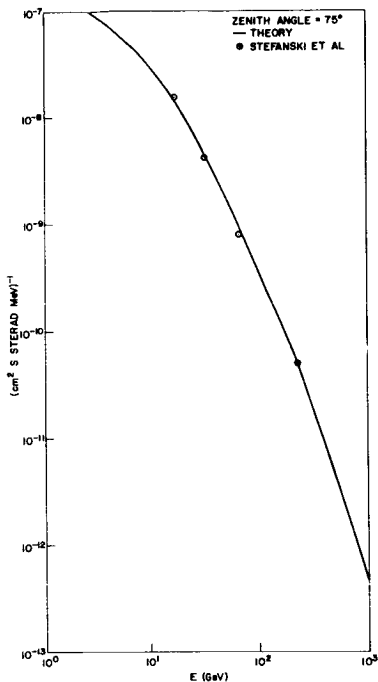
Fig. 8. The muon spectrum at a zenith angle of 75° as measured by Stefanski et al. (ref. 38) and as calculated.

Cosmic-Ray Ionization in the Atmosphere

Ionization from protons, pions and muons is calculated by multiplying the energy distributions by the appropriate stopping powers as described earlier (ref. 1). The lower energy limit for the proton, charged pion and neutral pion energy distributions is 100 MeV, below which the theory fails. The muons are allowed to slow down to 10 MeV, below which very little is contributed to the ionization.

It was found necessary empirically to use an upper limit of 10^4 GeV to include all significant contributors to the ionization.

In Fig. 9, the calculated ionization (in units of I, the number of ion pairs per cm^3 of NTP air) at a geomagnetic latitude of 55° is compared with the measurements of Neher (ref. 28), and later data as reported by George (ref. 39) down to 600 g/cm^2. To complete the curve, the results of Lowder and Beck (ref. 40) from 600 g/cm^2 to sea level measured at 51° geomagnetic latitude at about the same time are included.
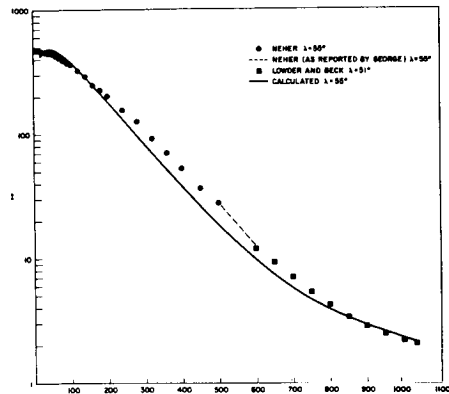

Fig. 9. The cosmic-ray ionization profile at 55° as measured by Neher (ref. 28) and by Lowder and Beck (ref. 40), and as calculated.

Over-all agreement is seen to be within 20% with the exception of the region near 600 g/cm^2, where the disagreement is nearer 40%. The comparison is absolute it must be emphasized. The composition of the total ionization is shown in Fig. 10. Because the secondary fluxes interact differently with the atmosphere each component has a noticeably different profile. The kink in the electron curve about 850 g/cm^2 is a consequence of the transition from shower production originating in neutral pion decay at low depths to shower production resulting from muon decay at larger depths.
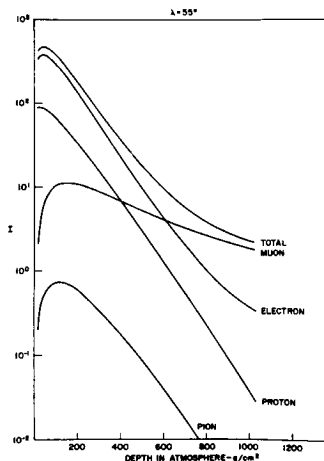

Fig. 10. The composition of cosmic-ray ionization in the atmosphere at 55°.

A similar comparison is shown in Fig. 11, where the calculation is carried out at 44°, and the data again are taken from Neher (ref. 28). To complete the curve, the data of George (ref. 39) are included from 188 g/cm² to sea level. The disagreement is typically 20% with higher values at near 800 g/cm² and 50 g/cm². The latter is probably a result of the departure of the incident primary cosmic-ray flux from isotropy, and the hardening of the photon production spectrum that results from the higher average cutoff (see Fig. 4). George's (ref. 39) measurements were carried out during 1968 near a solar maximum, and hence the additional modulation, if removed, would make the disagreement worse.
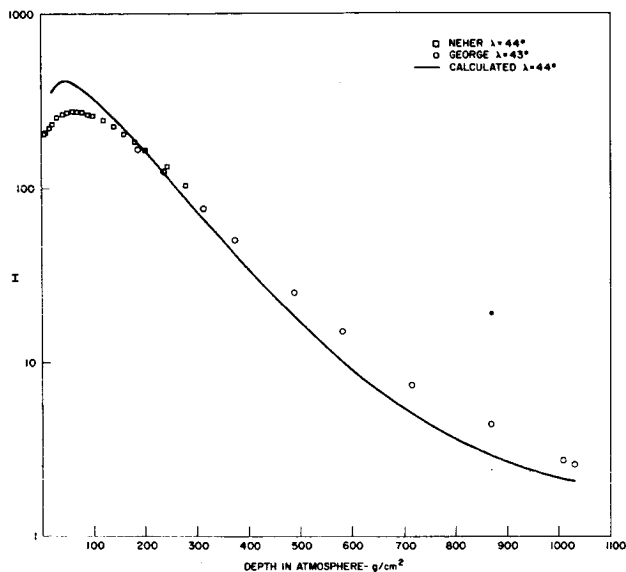

Fig. 11. The cosmic-ray ionization profile at 44° as measured by Neher (ref. 28) and by George (ref. 39) and as calculated.

Cosmic-Ray Neutrons in the Atmosphere

The lower energy limit of the cascade calculations described above is 100 MeV, and the agreement with measurement indicates that this cutoff which is forced on the calculations by the limitations of the analytical theory, is adequately high. This is a consequence of charged particle stopping which limits the number of charged particles at low energies. Neutrons are uncharged however, and extend all the way down to thermal energies. In order to account for neutron fluxes below 100 MeV, the cosmic-ray neutron spectrum reported by Hess et al. (ref. 41) at sea level and 44° geomagnetic latitude has been patched onto the calculated differential spectrum at 100 MeV. This approach is rather rude, and fails at small depths as it cannot account for the diffusion hardening which takes place near a vacuum boundary.

This is clearly seen in Fig. 12, where the neutron flux measurements of Boella et al. (refs. 42, 43), and Yamashita et al. (ref. 44) are compared with calculations. At depths greater than 200 g/cm² the agreement is really rather good. The lack of isotropy of the incident flux near cutoff and the absence of diffusion hardening lead to an overestimate at small depths. The measurements of Boella et al. (ref. 42) and Yamashita et al. (ref. 44) are both ground level measurements rather than free air measurements, but yet are seen to fall on the curve. The effect of the air ground interface on the calculations has not been evaluated.
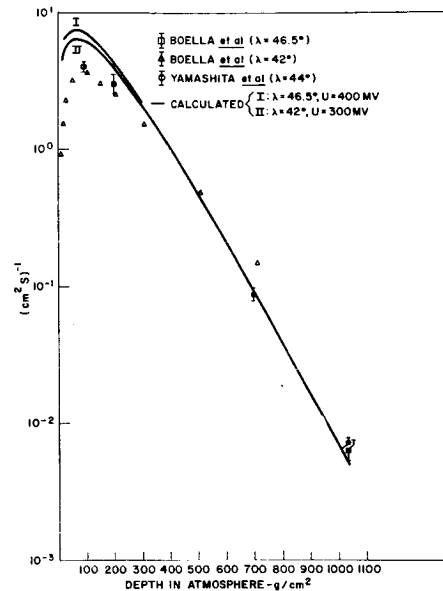

Fig. 12. The cosmic-ray neutron flux in the atmosphere as measured by Boella et al. (ref. 42), Boella et al. (ref. 43), and Yamashita et al. (ref. 44), and as calculated.

In Fig. 13, the neutron density measurements of Yuan (ref. 45) and Gold (ref. 46) have been compared with calculations on the same basis. Again, the agreement between calculations and measurements is good except at small depths, with the exception of the ground level value of Gold (ref. 46). Gold (ref. 46) recognizing that his values were quite high compared with balloon measurements in free air (ref. 47) attributed this to the interface with the ground, to which the neutron density appears much more sensitive than the neutron flux.

Yuan's data appear to have a markedly different slope from the measurements. This can also be seen in Boella et al. (ref. 43) on Fig. 12. This effect may be a consequence of operating near the threshold of instrument sensitivity since

936

the calculation is in good agreement with
the deeper measurements, all the way down
to sea level both in Fig. 5 and 12.   Such
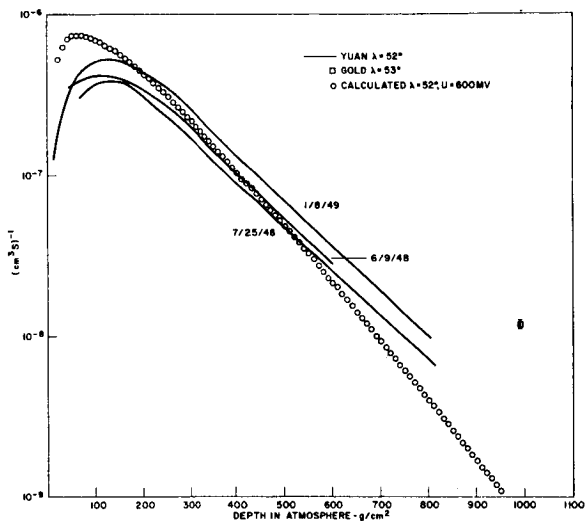an effect will lead to rather long
reported relaxation lengths.

Fig. 13. The cosmic-ray neutron density in the
atmosphere as measured by Yuan (ref. 45), and
Gold (ref. 46), and as calculated.

Fig. 14. The cosmic-ray neutron density in the
atmosphere as measured by Miles (ref. 48), and
as calculated.

Figure 14 shows the data of Miles
(ref. 48).   In this case a general under-
estimate appears below 200 g/cm^2.   The
identical calculations can be applied to
the data of Haymes (ref. 49) and Soberman
(ref. 50) which have been converted to
neutron density and adjusted by Miles
(ref. 48) for differences in latitude and
time so that comparison with his own re-
sults might be made.   Above 100 g/cm^2, the
data of Soberman (ref. 50) in Fig. 15 are
seen to be in excellent agreement with
calculation.   At smaller depths, the
neglect of leakage, which was not taken
into account in the low energy model,
causes the calculation to be too high.
Although much more scatter appears in the
measurements of Haymes (ref. 49), agree-
ment is clearly reasonably good except
again at small depths.

DISCUSSION

Analytical calculations of the
secondary energy distribution of cosmic-
rays in the atmosphere, cosmic-ray ioniza-
tion, and neutron flux and density have
been performed.   The model of nucleon-
nucleus collisions on which the calcula-
tions depend is based on the constant
partial inelasticities of Table I, and
constant geometric reaction cross sections.
The transport calculations assume a purely
nucleonic cascade, and consider (eq. 5)
only protons, neutrons, pions, electrons
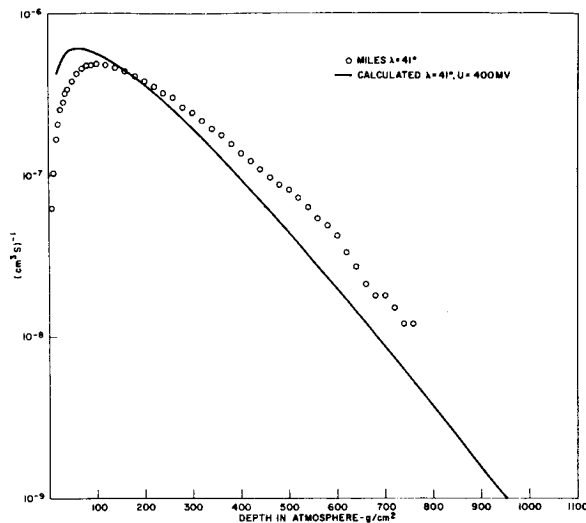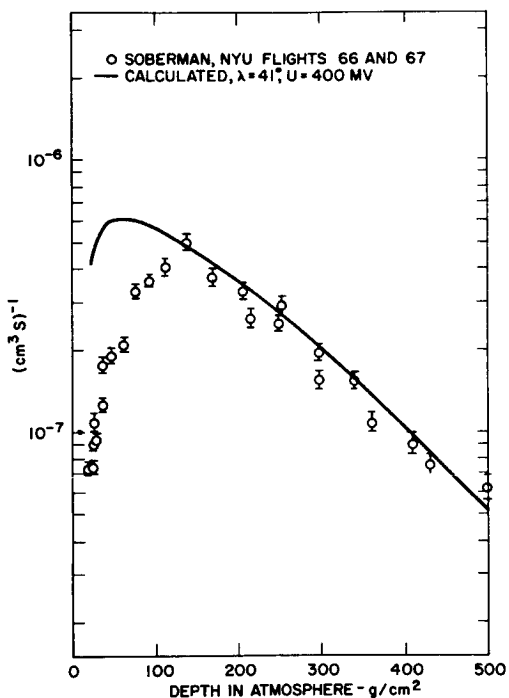and photons.

Fig. 15. The cosmic-ray neutron density in the
atmosphere as measured by Soberman (ref. 50),
and adapted by Miles (ref. 48), and as
calculated.

In particular; the muon ionization
and the high zenith angle energy distri-
butions calculated on the basis of $\pi^{\pm} \to \mu$
decay, are in agreement with measurement
(Fig. 8) and support the conclusion of
Stefanski et al. (ref. 38) that there is
no other important contribution to the
muon flux below 300 GeV such as would
account for the Utah muon measurements
(ref. 51).

Ranft and Borak (ref. 9) observe that the measurements of negative pions at 70 GeV of Bushnin et al. (ref. 52) are in strong disagreement with the TRB model of hadron nucleus collisions and with the statistical model of strong interactions (ref. 3). The extrapolation model disagrees by an order of magnitude with the same data (ref. 8). If the measurements are correct, they cannot imply a change in the appropriate partial inelasticities. As has been shown the power law model used in the calculations of the fluxes in figs. 5-8 is in agreement with these models. Thus a large error in the assigned values of ν_j or K_j would lead to quite large errors in the differential nucleon, pion and muon fluxes starting somewhere between 30 and 70 GeV. However, the measurements are only at small angles ($\leq$ 15 milliradians) and high secondary momenta (> 45 GeV/c), and it is possible that average quantities such as multiplicity and inelasticity are not much affected by what happens in this region.

It has been suggested that nucleon-nucleon and meson-nucleon cross sections may vanish at infinite energy (ref. 53). These calculations, performed with constant cross sections, indicate that hadron-nucleus cross sections are essentially constant and geometric out to 10^4 GeV. For instance, a 10% perturbation of the nucleon-nucleus cross section will cause a change in the nucleonic flux in the region of 10^3 - 10^4 GeV of 150%. This would put theory and experiment out of agreement in Fig. 5. But, such a discrepancy could be accounted for in terms of errors in the primary spectrum used, or errors in the sea level measurements. Much larger changes in the cross section however, would lead to very big changes in the sea-level flux which would not be reconcilable with the data.

In these calculations, all hadron-nucleus cross sections are equal and geometric. It is known that pion-nucleon cross sections are 2/3 of the nucleon-nucleon cross sections (ref. 53). As Adair (ref. 18) points out, pion-nucleus and nucleon-nucleus cross sections will differ by less than this as a consequence of the intra-nuclear cascade. He calculates the ratio to be 0.77. Ranft and Borak (ref. 9) obtain 0.83 from published experimental data. The effect on pion and muon spectra of a 20% error in the reaction cross section would be much less than in the nucleon case, as pions are locally produced, and locally absorbed.

Apparently one-dimensional nucleonic cascades depend only weakly on the angular and energy behavior of the secondary production spectra, but strongly on the partial inelasticities, multiplicities and cross sections. The calculation described here which is based on a straight ahead power law approximation to the doubly differential production spectrum yields good agreement with the sea level differential fluxes of nucleons, pions and muons, with the cosmic-ray ionization at all depths in the atmosphere, and with the neutron fluxes and densities in the atmosphere.

Lastly, it may be observed that in Figs. 12, 13, and 14, the neutron calculations appear to relax more rapidly than some sets of measurements. Yet in the Fig. 5, and the sea level values of Fig. 12, this would appear to represent experimental error, possibly a consequence of operating near the threshold of experimental sensitivity. Too rapid a relaxation rate of the nucleon spectrum would also result in the calculated pion spectrum of Fig. 6 to be too low, which it is not, as the pions are produced locally from nucleon-nucleus collisions.

The neutron attenuation is not actually exponential although its departure from exponentiation is not large (ref. 54). In Table IV, relaxation lengths obtained from the neutron density calculations at $\lambda = 41^0$ and with U = 400 MV are compared with Miles (ref. 47). Agreement is poor, but the calculated neutron densities agree well with Haymes (ref. 49) and Soberman (ref. 50) when they are reduced to the same conditions and are never less than half of Miles (ref. 49). In addition, Simionati deFritz and Cicchini (ref. 54) have measured cosmic-ray neutron attenuation lengths in air at 25^0 (ref. 55) as a function of atmospheric depth which are included for comparison. In this case agreement is quite close, and this suggests that exponential relaxation lengths are not well determined by experimental attenuation data, as relaxation rates are not constant with height and the true variation is marred by poorer quality at greater depths and at lower intensities.

The success of the preceding calculations rests primarily on the phenomenological model of hadron-nucleus collisions presented here. The description of the exclusively nucleonic cascade combined with the neglect of kaons is a simplification with which more sophisticated and expensive calculations may dispense. Other, more obvious, approximations are being discarded as the study progresses.

Real improvement on the forms of the doubly differential production spectra must probably await progress in studies being carried out at Oak Ridge and elsewhere. The adequacy of the power law nuclear model for calculations of this type is clear from the results shown here, and the average properties, particularly the partial inelasticities and cross sections, as applied to air, appear to be well established.

Table IV. – Comparison of calculated neutron attenuation lengths for $\lambda = 41^\circ$ and U = 400 MV with measurements.

Atmospheric depth (g/cm^2)	Calculated (g/cm^2)	Measured (g/cm^2)
300	149	155[a]
500	129	125[a], 165±20[b]
1033	113	115[a]

[a] $\lambda = 25^\circ$ (ref. 54).
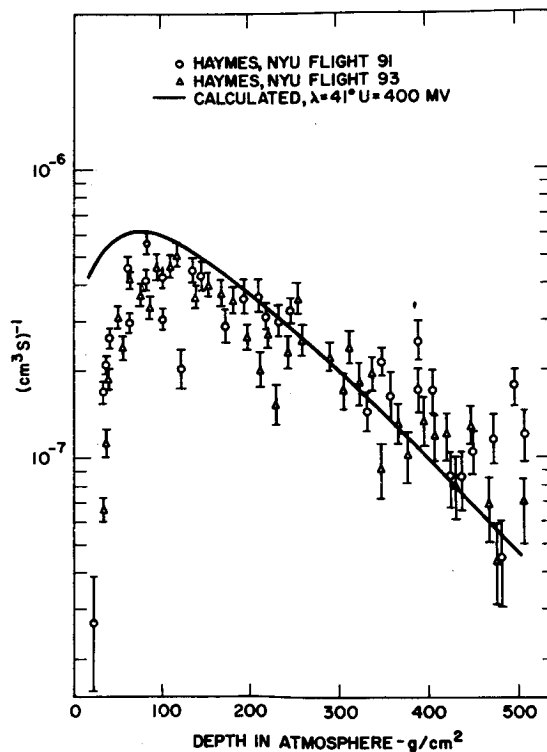
[b] $\lambda = 41^\circ$ (ref. 47).

Fig. 16. The cosmic-ray neutron density in the atmosphere as measured by Haymes (ref. 49) and adapted by Miles (ref. 48), and as calculated.

REFERENCES

1. O'Brien, K.: J. Geophys. Res., vol. 75, 1970, p. 4357.
2. Fujimoto, Y.; and Hayakawa, S.: Cosmic rays and high-energy physics, in Encyclopedia of Physics, 46/2, Springer-Verlag, Berlin, 1967, p. 115.
3. Hagedorn, R.; and Ranft, J.: Nuovo Cimento Suppl., vol. 6, 1968, p. 169.
4. Alsmiller, R. G., Jr.; and Barish, J.: ORNL-3855, 1965.
5. O'Brien, K.: Nucl. Instr. and Meth., vol. 72, 1969, p. 93.
6. Cocconi, G.; Koester, L. J.; and Perkins, D. H.: UCRL-10022, 1961, p. 167.
7. Trilling, G.: Lawrence Radiation Laboratory Report, UCID-10148, 1966.
8. Gabriel, T. A.; Alsmiller, R. G., Jr.; and Guthrie, M. P.: ORNL-4542, 1970.
9. Ranft, J.; and Borak, T.: Improved nucleon-meson cascade calculations, FN-193,1100.0, National Accelerator Laboratory, 1969.
10. Camerini, U.; Davies, J. H.; Fowler, P. H.; Franzinetti, C.; Muirhead, H.; Lock, W. O.; Perkins, D. H.; and Yekutieli, G.: Phil. Mag., vol. 42, 1951, p. 1241.
11. Meyer, H.; Teucher, M. W.; and Lohrmann, E.: Nuovo Cimento, vol. 28, 1963, p. 1399.
12. Bertini, H. W.: Phys. Rev., vol. 188, 1969, p. 1711.
13. Alsmiller, R. G., Jr.; Alsmiller, F. S.; and Murphy, J. E.: ORNL-3289, 1963.
14. Alsmiller, R. G., Jr.; Alsmiller, F. S.; and Barish, J. B.: ORNL-3854, 1967.
15. Kronrod, S. A.: Nodes and Weights of Quardrature Formulas, Consultants Bureau, New York, 1965.
16. Passow, C.: Phenomenologische Theorie zur Berechnung einer Kaskade aus schweren Teilchen (Nukleonenkaskade) in der Materie, Desy Notiz A. 2.85 (1962), Deutches Elektronen Synchrotron, 1962.
17. Alsmiller, F. S.: ORNL-3746, 1965.
18. Adair, R. K.: Phys. Rev., vol. 172, 1968, p. 1370.
19. Armstrong, T. W.; and Alsmiller, R. G., Jr.: The nucleon-meson cascade in iron induced by 1 and 3 GeV protons, in ORNL-RSIC-25, ANS-SD-9, Shielding Benchmark Problems, A. E. Profio, ed., Oak Ridge National Laboratory, 1970.
20. O'Brien, K.: Nucl. Instr. and Meth., vol. 86, 1970, p. 217.
21. Zerby, C. D.; and Moran, H. S.: ORNL-3320, 1962.
22. Beck, H.: USAEC Report HASL-213, 1969.
23. Gleeson, L. J.; and Axford, W. I.: Can. J. Phys., vol. 46, 1968, p. S937.
24. Freier, P. S.; and Waddington, C. J.: Space Science Reviews, vol. 4, 1965, p. 313.
25. Ehmert, A.: Proceedings of the International Conf. on Cosmic Rays, Moscow 1959, vol. 4, 1960, p. 140.
26. Freier, P. S.; and Waddington, C. J.: Proceedings of the Ninth International Conf. on Cosmic Rays, London 1965, vol. 1, 1966, p. 176.
27. Peters, B.: Cosmic-rays, in Handbook of Physics, eds. E. U. Condon and H. Odishaw, McGraw-Hill, New York, 1958, p. 9.
28. Neher, H. V.: J. Geophys. Res., vol. 72, 1967, p. 1527.
29. Richtmeyer, F. K.; Kennard, E. H.; and Lawritsen, T.: Introduction to Modern Physics, (5th Edition), McGraw-Hill, New York, 1955, p. 566.
30. Lemaitre, G.; and Vallarta, M. S.: Phys. Rev., vol. 50, 1936, p. 493.

31. Brook, G.; and Wolfendale, A. W.: Proc. Phys. Soc., vol. 83, 1964, p. 843.

32. Ashton, F.; and Coats, R. B.: J. Phys. A (Proc. Phys. Soc.), vol. 1, 1968, p. 169.

33. Brooke, G.; Meyer, M. A.; and Wolfendale, A. W.: Proc. Phys. Soc., vol. 83, 1964, p. 871.

34. Owen, B. G.; and Wilson, J. G.: Proc. Phys. Soc., vol. 68, 1955, p. 409.

35. Holmes, J. E. R.; Owen, B. G.; and Rodgers, A. L.: Proc. Phys. Soc., vol. 78, 1961, p. 505.

36. Gardener, M.; Jones, D. G.; Taylor, F. E.; and Wolfendale, A. W.: Proc. Phys. Soc., vol. 80, 1962, p. 697.

37. Hayman, P. J.; and Wolfendale, A. W.: Proc. Phys. Soc., vol. 80, 1962, p. 110.

38. Stefanski, R. J.; Adair, R. K.; and Kasha, H.: Rev. Letters, vol. 20, 1968, p. 950.

39. George, M.: J. Geophys. Res., vol. 75, 1970, p. 3693.

40. Lowder, W. M.; and Beck, H. L.: J. Geophys. Res., vol. 71, 1966, p. 4661.

41. Hess, W. N.; Canfield, E. H.; and Lingenfelter, R. E.: J. Geophys. Res., vol. 66, 1961, p. 665.

42. Boella, G.; Degli Antoni, G.; Dilworth, C.; Gianneli, G.; Rocco, E.; Scarsi, L.; and Shapiro, D.: Nuovo Cimento, vol. 29, 1963, p. 103.

43. Boella, G.; Degli Antoni, G.; Dilworth, C.; Panetti, M.; Scarsi, L.; and Intriligator, D. S.: J. Geophys. Res., vol. 70, 1965, p. 1019.

44. Yamashita, M.; Stephens, L. D.; and Patterson, H. W.: J. Geophys. Res., vol. 71, 1966, p. 3817.

45. Yuan, C. L.: Phys. Rev., vol. 81, 1951, p. 175.

46. Gold., R.: Phys. Rev., vol. 165, 1968, p. 1411.

47. Miles, R. F.: J. Geophys. Res., vol. 69, 1964, p. 1277.

48. Miles, R. F.: Thesis, California Institute of Technology, 1963.

49. Haymes, R. C.: Phys. Rev., vol. 116, 1959, p. 1231.

50. Soberman, R. K.: Phys. Rev., vol. 102, 1956, p. 1399.

51. Bergeson, H. E.; Keuffel, J. W.; Larson, M. O.; Mason, G. W.; and Osborne, J. L.: Phys. Rev. Letters, vol. 21, 1968, p. 1089.

52. Bushnin, Y. B.; Denisov, S. P.; Donskov, S. V.; Dunaitsev, A. F.; Gorin, Y. P.; Kachanov, V. A.; Khodirev, Y. S.; Kotov, V. I.; Kutyin, V. M.; Petrukhin, A. I.; Prokoshkin, Y. D.; Razuvaev, E. A.; Shuvalov, R. S.; Stoyanova, D. A.; Allaby, J. V.; Binon, F.; Diddens, A. N.; Duteil, P.; Giacomelli, G.; Meunier, R.; Peigneux, J.-P.; Schlupmann, K.; Spighel, M.; Stahlbrandt, C. A.; Stroot, J.-P.; and Wetherell, A. M.: Phys. Letters, vol. 29B, 1969, p. 48.

53. Wetherell, A. M.: Selected Topics in Particle Physics, ed., J. Steinberger, Academic Press, New York, 1968.

54. Simionati deFritz, N. A.; and Cicchini, A. A.: Nuovo Cimento, vol. 40B, 1967, p. 220.

55. McNish, A. G.: Terrest. Magnetism Atmospheric Elec., vol. 41, 1936, 37.